Journal of Neonatal Surgery
ISSN(Online): 2226-0439
Vol. 14, Issue 15s (2025)
https://www.jneonatalsurg.com

OPEN ACCESS

Polymeric Nanoparticles in Oncology: Design, Development and Characterization

Sonali Gurav[1*], Dr. Anshu Sharma[2], Sunita Shinde[3], Raju Rathod[4]

Research Scholar, Bhupal Nobels University, Udaipur, 313001

[2]Faculty of Pharmacy, Bhupal Nobels University, Udaipur, 313001

[3]Assistant Professor, Tatyasaheb Kore College of Pharmacy, Warananagar.

[4]Assistant Professor, Shree Ambabai Talim Sanstha's, Diploma In Pharmacy College, (Affiliated to DBAT University) Miraj. 416410

***Corresponding Author:**

Ms. Sonali Gurav

Bhupal Nobels University, Udaipur, Rajasthan. 313001

Email ID: ssdgurav.tkcp@gmail.com

Cite this paper as: Sonali Gurav, Dr. Anshu Sharma, Sunita Shinde, Raju Rathod, (2025) Polymeric Nanoparticles in Oncology: Design, Development and Characterization. *Journal of Neonatal Surgery*, 14 (15s), 615-637.

ABSTRACT

Non-small cell lung cancer (NSCLC) treatment is often limited by the poor aqueous solubility and systemic side effects of Erlotinib, an EGFR inhibitor. To overcome these challenges, this study explores the use of β-Cyclodextrin (BCD), a natural polymer, for the development of biodegradable polymeric nanoparticles to enhance drug solubility, bioavailability, and therapeutic efficacy. Erlotinib-loaded BCD-based nanoparticles were formulated using High-Pressure Homogenization (HPH) and characterized for particle size, polydispersity index (PDI), zeta potential, drug encapsulation efficiency, and in vitro drug release kinetics. Additionally, their cytotoxicity against NSCLC cell lines, biocompatibility, and pharmacokinetic behavior were evaluated. The optimized formulation (Batch B10) demonstrated high drug encapsulation efficiency, controlled and sustained release, and enhanced solubility due to the inclusion of BCD. The nanoparticles exhibited suitable physicochemical properties for targeted delivery, with improved stability and dissolution behavior. In vivo pharmacokinetic studies confirmed a significant increase in bioavailability, with Batch B10 showing superior systemic absorption compared to pure Erlotinib. The study confirms that BCD, a natural polymer, plays a crucial role in enhancing Erlotinib solubility, bioavailability, and therapeutic effectiveness. The optimized BCD-based nanoparticles offer a promising strategy for improving NSCLC treatment while potentially reducing dose-related side effects.

Keywords: *Non-small cell lung cancer, Erlotinib, β-Cyclodextrin, biodegradable nanoparticles, targeted drug delivery, bioavailability, controlled release.*

1. INTRODUCTION

A major challenge in the development of novel drug delivery systems is ensuring the stability of the formulation. Many drugs, particularly those classified under BCS Class II, exhibit low solubility, which limits their bioavailability. This issue can be effectively addressed using biodegradable polymeric nanoparticles, a promising approach in modern pharmaceutical research. According to recent literature, biodegradable polymeric nanoparticles offer greater stability and cost-effectiveness compared to other nanoparticle formulations. Their application in cancer drug delivery has been extensively explored due to their ability to enhance drug solubility and controlled release. Erlotinib, a potent anticancer drug, is an ideal candidate for this approach. Its incorporation into biodegradable polymeric nanoparticles can improve its therapeutic efficacy, making it a suitable choice for the present study. [1]

Cancer remains a leading cause of mortality worldwide, characterized by uncontrolled cell proliferation, invasion, and metastasis. Despite advancements in conventional therapies such as surgery, radiation, and chemotherapy, significant challenges persist, including poor drug solubility, off-target toxicity, and multidrug resistance. These limitations necessitate the development of **novel drug delivery systems** to enhance therapeutic efficacy while minimizing systemic side effects. Cancer starts when the cells start growing rapidly and crowding of cells occur which is more than the normal cells. There are different causes of cancer and there exists various kinds of cancer which depend on the kind of tissue and the

primary site of the cancer. Lung Cancer seems to be a most unique type of cancer as the most important etiologic agent is nothing but a very addictive product which is produced and promoted by the industry itself. It is seen and proven that Cigarette smoking is the most frequent cause of lung cancer. A projected 238,340 individuals (120,790 women and 117,550 men) will receive a lung cancer diagnosis in 2023, and 127,070 of them will pass away from the illness. Globally,>1.5 million people die with lung cancer annually. In light of the American Cancer Society's estimations for lung cancer Based on data from 2020, the United States has around 228,820 new cases of lung cancer and 135,720 lung cancer-related deaths. The United States is expected to have 2,001,140 new cases of cancer and 611,720 cancer-related deaths in 2024. [2]

Nanoparticles (NPs) are particles between 1 to 100 nm in size used as to change, improve pharmacokinetic and pharmacodynamics properties of drug molecules. Due to their small sizes, the nanostructures exhibit unique physicochemical and biological properties that make them a favorable material for biomedical applications. NPs formation systems are useful for improving drug solubility, stability, absorption and bioavailability. While convert in NPs decrease in size of particles which increases surface area of particles and this in turn increases the dissolution rate by the Noyes Whitney equation. Preparation of NPs by various methods which are solvent evaporation technique, nano-precipitation technique, solvent diffusion technique dialysis technique, high pressure homogenization technique (HPH).[3]

This project involves a comprehensive investigation into the selection, formulation, characterization, and optimization of polymeric nanoparticles to enhance drug delivery and therapeutic efficacy. The initial phase focuses on identifying suitable biodegradable polymers by evaluating their biocompatibility, drug loading capacity, and controlled release properties. By analyzing different polymers, the objective is to determine the most effective candidates for encapsulating Erlotinib. The formulation process employs techniques such as nanoprecipitation, emulsification, and solvent evaporation, aiming to optimize key parameters like particle size, drug encapsulation efficiency, and nanoparticle stability. By systematically investigating these aspects, this project aims to advance nanomedicine-based strategies for NSCLC therapy. The ultimate goal is to improve patient outcomes, enhance drug efficacy, and minimize side effects, thereby contributing to the evolution of targeted cancer treatments. The integration of biodegradable polymeric nanoparticles into clinical applications holds promise for revolutionizing lung cancer therapy by offering a more effective, patient-friendly approach to treatment. [4]

2. METHODOLOGY

2.1 Materials

The kind donation of Erlotinib came from Sakar Healthcare Ltd., Gujarat. While PLGA was purchased from Ashl and Specialties Irel and Ltd., Ireland, β – cyclodextrin and Poloxamer407 was purchased from Fine Chemical, Mumbai. Mumbai-based Fine Chemical, Mumbai provided Methanol and Acetone high purity and analytical grade were guaranteed for all other compounds utilized in the investigation.

2.2 Experimental Design

A **3^2 Box-Behnken Design (BBD)** was employed to evaluate the combined effect of two key formulation variables, each at three levels, resulting in **15 different formulations** of **Erlotinib-loaded polymeric nanoparticles**. The **Drug:** β-cyclodextrin **batch** was specifically chosen for this study due to its **smaller particle size (Z-average: 111.1 nm, PDI: 0.239)**, which enhances the potential for optimization through statistical modeling. The independent variables selected were **Drug quantity (X_1),** β-cyclodextrin **(X_2), and HPH cycle (X_3)**, while the **dependent response variables** included **Particle Size (Y_1) and Entrapment Efficiency (Y_2)**. The application of **high-pressure homogenization (HPH), previously identified as the most effective nanoparticle preparation method**, ensured uniform and stable nanoparticle dispersion, making the Drug: β-cyclodextrin batch ideal for further **DOE-based optimization** to refine formulation parameters. The **15 formulations** were prepared and analyzed, and the resulting data were processed using **Design Expert software (Tech Expert 13, Stat-Ease)**. **Analysis of Variance (ANOVA)** was conducted to validate the experimental design. The generated polynomial equations allowed for interpretation based on the **magnitude and sign of the coefficients**, facilitating an understanding of the influence of each independent variable on the responses.

2.2.1 Generation of polynomial equations

We performed various computations in the context of our present optimization study utilizing Response Surface Methodology (RSM) and Design Expert software Trial version 11.0. Using a Multiple Linear Regression Analysis (MLRA) technique, we created polynomial models that included interactions for all of the response variables.

2.2.2 Statistical analysis of data

To analyses the impact of independent factors on answers, we used statistical analytical methods, specifically analytical of Variance (ANOVA) in Design Expert software (version 11.0). The threshold for statistical significance was set at $p>0.05$.

2.2.3 Generation of 3D response surface plots

To visualize the responses we measured, we created three-dimensional plots that illustrate how the response surface changes.

These plots are valuable tools for examining how two factors simultaneously affect a response. They provide a graphical representation of how independent variables influence the responses. [5]

2.2.4 Formulation of Nanoparticles

High-Pressure Homogenization (HPH) -

The polymer was dissolved in an appropriate **organic solvent** and emulsified into an **aqueous surfactant solution** under continuous stirring. The resulting emulsion was then subjected to **high-pressure homogenization** using the **GEA NIRO SOAVI Panda Plus** under controlled **pressure cycles** to reduce droplet size and improve nanoparticle uniformity. The processed emulsion was then **evaporated under reduced pressure** to remove the organic solvent. The composition of formulation are shown in the table 9. [6, 7]

3. CHARACTERIZATION OF NANOPARTICLES

3.1 Entrapment Efficiency

The entrapment efficiency of **Erlotinib-loaded β-Cyclodextrin and Poloxamer nanoparticles** was determined using the centrifugation method. The nanoparticle suspensions were transferred into centrifuge tubes and centrifuged at **8,000 rpm for 30 minutes** at room temperature to separate the free drug from the encapsulated drug. The supernatant was collected and suitably diluted with **methanol**. [8] The concentration of the unencapsulated drug was quantified using **UV-Visible spectroscopy at 244 nm**. The Entrapment efficiency was calculated by using the formula,

$$\%\ \boldsymbol{Entrapment\ efficiency} = \boldsymbol{Total\ amount\ of\ drug - Drug\ in\ supernatant\ /Total\ amount\ of\ drug\ x}\ \mathbf{100}$$

3.2 Particle Size and Polydispersity Index

The mean particle size and size distribution of **β-Cyclodextrin and Poloxamer nanoparticles** were analyzed using **Dynamic Light Scattering (DLS) with a Zetasizer (Nano ZS, Malvern Instruments, UK)**. Samples were diluted with distilled water and measured at **25°C** to determine the **mean particle size, polydispersity index (PDI), and distribution profile**.[9]

3.3 Zeta Potential

The **zeta potential** of **Erlotinib-loaded β-Cyclodextrin and Poloxamer nanoparticles** was determined using a **Zetasizer (Nano ZS, Malvern Instruments, UK)** to evaluate the **surface charge and stability of the nanoparticle dispersions**. The analysis was performed at **25°C** in distilled water to measure electrostatic potential. [10]

4. LYOPHILIZATION OF OPTIMIZED BATCH

The **optimized batch** of Erlotinib-loaded polymeric nanoparticles was lyophilized using a **Virtis Freeze Dryer (USA)** to enhance its shelf life and evaluate its dissolution behavior. To prevent nanoparticle aggregation during the freeze-drying process, **1% w/v mannitol** was added as a cryoprotectant. The optimized nanoparticle suspension was pre-frozen at **-70°C overnight** in a deep freezer to ensure uniform freezing. The frozen sample was then subjected to **lyophilization in a Virtis freeze dryer** under vacuum conditions of **2 millitorr at -50°C for 48 hours**. The resulting lyophilized powder was collected and stored in an airtight container for further **characterization and dissolution studies**. This lyophilization process ensures **long-term stability, ease of handling, and improved reconstitution properties** of the optimized nanoparticle formulation. [11, 12]

5. EVALUATION OF OPTIMIZED LYOPHILIZED BATCH

5.1 Percentage Yield:-

The percentage yield of the optimized lyophilized batch was determined to evaluate the efficiency of the nanoparticle formulation process. The freeze-dried nanoparticles were carefully collected and weighed. [13] The percentage yield was calculated using the following formula:

Percentage Yield = (Practical Yield/ Theoretical Yield) × 100

5.2 Drug Content-

The drug content of the optimized batch was analyzed by dissolving a known amount of lyophilized nanoparticles in **methanol** and measuring the absorbance at **244 nm using UV-Visible Spectrophotometry**. The concentration of Erlotinib was determined using a pre-established calibration curve, and the drug content was expressed as a percentage of the theoretical drug amount. [14]

Drug Content (%) = (Actual Drug Content/Theoretical Drug Content) × 100

5.3 Saturation Solubility -

The saturation solubility of the optimized lyophilized batch was evaluated in **distilled water and phosphate buffer pH 7.4** using the **mechanical shaker method**. A known quantity of nanoparticles was dispersed in **10 mL of each solvent** and shaken at **37°C for 24 hours**. The samples were centrifuged, filtered, and analyzed using **UV-Visible Spectrophotometry at 244 nm** to determine the solubility of Erlotinib. [15]

5.4 Fourier Transform Infrared Spectroscopy (FTIR):

The chemical integrity and potential interactions of the optimized lyophilized formulation were evaluated using **Fourier Transform Infrared Spectroscopy (FTIR)**. The FTIR spectra were recorded using **FTIR (Cary-630, Agilent Technology)** over the wavenumber range of **4000–400 cm^{-1}**. The absorption spectra were analyzed to identify functional groups and detect any possible interactions between the drug and excipients. The observed peaks were compared with reference spectra to confirm the formulation's stability and purity. [16]

5.5 Powder X-Ray Diffraction (PXRD) Analysis:

Powder X-ray diffractometry (PXRD) is a vital analytical technique used to assess the crystallinity of pharmaceutical formulations. It helps in detecting crystalline phase constituents and identifying any structural modifications that may affect the drug's stability and therapeutic efficacy. The PXRD analysis was conducted on the **optimized lyophilized batch** to evaluate changes in crystallinity following nanoparticle formulation. The **X-ray diffraction patterns** of **pure Erlotinib and its polymeric nanoparticle suspension** were recorded using an **X'Pert PRO MPD diffractometer (PANalytical, Netherlands)**. The system was equipped with a **2.2 kW copper anode** as the X-ray source, and data acquisition was performed using a **LynxEye detector**. A **Ni filter** was employed to refine the diffraction pattern. The obtained diffractograms were analyzed to compare the crystallinity of the pure drug and the formulated nanoparticles, assessing the impact of the nanoparticle formulation process. [17, 18]

5.6 Differential Scanning Calorimetry (DSC) Study:

Differential Scanning Calorimetry (DSC) is a crucial analytical technique used in the pharmaceutical industry to assess the thermal properties, purity, crystallinity, stability, and compatibility of drug substances and excipients. It provides essential information about melting behavior, glass transition temperature, and possible drug-excipient interactions, which can significantly influence the formulation's performance and stability. For this study, DSC analysis of the optimized batch was carried out using a Shimadzu DSC-60 system with TDA Trend Line software (Shimadzu Corporation, Japan). The thermal behavior of pure Erlotinib and its polymeric nanoparticles was evaluated by heating the samples at a controlled rate of 10°C/min under a nitrogen atmosphere to prevent oxidative degradation. The thermograms obtained were analyzed to detect changes in crystallinity, confirm successful drug entrapment within the polymeric matrix, and assess any thermal transitions that could impact formulation stability. Although a minimum purity of 98% is required for DSC measurements, this technique alone is not sufficient to determine purity but serves as a valuable complementary method for comprehensive thermal characterization. The findings from DSC analysis provide critical insights into the physicochemical stability and structural integrity of the optimized polymeric nanoparticle formulation, ensuring its suitability for further pharmaceutical applications. [19, 20]

5.7 Scanning Electron Microscopy (SEM) Analysis:

The morphological characteristics, surface topology, and particle size distribution of the optimized Erlotinib-loaded polymeric nanoparticles were examined using Scanning Electron Microscopy (SEM) (Model INC Awave). This technique provides high-resolution imaging to evaluate the shape, surface smoothness, and aggregation tendency of nanoparticles, which are critical parameters influencing drug delivery efficiency. For SEM analysis, the nanoparticle samples were carefully mounted on a rigid bronze specimen holder, known as a specimen stub, using a double-sided adhesive carbon tape to ensure stability during imaging. To enhance electron conductivity and prevent surface charging, the samples were coated with an ultrathin layer of gold using a sputter coater under low vacuum conditions or by high-vacuum evaporation. This gold coating ensures clear imaging and accurate visualization of nanoparticle surface morphology under the electron beam.[20]

***5.8 In-Vivo* Study of optimized batch -**

The pharmacokinetics of Erlotinib and optimized batch B10 were evaluated in a fasted SD rat model. Animals Albino rat (Wistar strain) (SD) rats) of 200–250 g were obtained in Biocytes lab Sangli, Maharashtra India. The study protocol was approved by the Institutional Animal Ethics Committee (IAEC), National Institute of Pharmaceutical Education and Research (NIPER), S.A.S Nagar, India. The animals were maintained at 25 ± 2°C and 50–60% relative humidity under natural light/dark conditions for one week before the experiment. Rats were divided into two groups (n = 5). A dose of 10 mg/kg dose of Erlotinib was orally administered to one group while the other group received optimized batch B10 equivalent to 10 mg/kg of Erlotinib. The animals were fasted overnight (at least 8 h before dosing). The individual dose was calculated based on body weights measured on the day of drug administration. Blood samples were collected via retro-orbital venipuncture into heparinized tubes at regular time interval for upto 24 h. Blood samples were centrifuged at 10,000 rpm for 10 min. The plasma samples were collected and stored at −20 °C until analyzed.

The plasma samples were analyzed for Erlotinib concentrations using in-housed developed and validated reverse phase HPLC method.

The study will involve male albino rats of the Wistar strain, aged 6-8 weeks and weighing between 200-250 grams. A total of 10 rats will be used, with a yearly breakdown of usage and total figures provided in tabular form as per the requirements. The rats will be housed for a duration according to the specific needs of the study. For the injections schedule, the substance will be administered orally at a dose of 10 mg/kg, once per day. Blood samples will be withdrawn through the retro-orbital route, with a volume of 1-2 ml per animal. [21, 22]

6. RESULTS AND DISCUSSION

6.1 Data Optimization:

Data Analysis:

The three levels and two Box Behnken designs have effective approaches for determining variables at limited numbers of trials runs with different levels (Table 8.12). The particle size and Entrapment Efficiency are total numbers of 15 batches showed extensive variations from 169.6 to 290.6 nm and 65 to 82 % respectively. [23]

Effect of formulation variables:

Response 1: Particle Size

The full model statistical analysis showed in Table 1 and shows that the independent variables have a considerable impact on the responses.

Analysis of Variance (ANOVA), pure error, lack of fit and fit statistics:

Table 1:- Sources and R value

"Source	Sequential P- value	Adjusted R	Predicted R
Linear	0.0202	0.4602	0.0776
2 FI	0.4059	0.5078	-1.1188
Quadratic	0.4039	0.5078	-2.0623"

Table 2:- ANOVA for 2FI

"Source	Sum of squares	Df	Mean square	F- value	P- value"
Model	1.607E+05	3	53554.9	4.98	0.0202
A-Drug	9449.48	1	9449.48	0.8785	0.3687
B-B	40896.02	1	48896.02	3.80	0.0771
HPH cycle	1.103E+05	1	1.103E+05	10.26	0.0084
Residual	1.183E+05	1	10756.40	-	-
C or total	2.790E+05	14	-	-	-

The Model F-value of 4.98 implies the model is significant. There is only a 2.98% chance that an F-value this large could occur due to noise. P-values less than 0.0500 indicate model terms are significant. In this case B, AC is significant model terms. Values greater than 0.1000 indicate the model terms are not significant. If there are many insignificant model terms (not counting those required to support hierarchy), model reduction may improve your model. The Lack of Fit F-value of 0.03 implies the Lack of Fit is not significant relative to the pure error. There is a 99.93% chance that a Lack of Fit F-value this large could occur due to noise. Non-significant lack of fit is good - we want the model to fit. Fit Statistics for Particle Size. [24, 25]

Table 3:- Fit Statistics for Particle size

Std. Dev.	103.71	R^2	0.5759
Mean	217.87	Adjusted R^2	0.4602
C.V.%	47.60	Predicted R^2	0.0776
-	-	Adeq Precision	7.2296

The Predicted R^2 of 0.0776 is in reasonable agreement with the Adjusted R^2 of 0.4602; i.e. the difference is less than 0.2 Adeq. Precision measures the signal to noise ratio. A ratio greater than 4 is desirable. [26] Your ratio of 7.220 indicates an adequate signal. This model can be used to navigate the design space.

Table 4:- Particle size ratio

Particle size	= +210.07
-30.74	A
-.63.95	B
-87.75	C

Predictions can be made regarding the reaction to different levels of each ingredient by utilizing an equation that is represented in terms of the coded factors. Typically, the factors with high levels are given a value of +1, while the factors with low levels are given a value of -1. The relative impact of the components can be determined by comparing the factor coefficients, which is a valuable application of the coded equation. [27]

Contour Plots and 3D Surface Analysis:

Two-dimensional contour plots and three-dimensional response surface plots are presented in figures 1& 2 which are very useful to study the interaction effects of the factors on the responses. These categories of plots are helpful in simultaneously observing the effect of two variables on these responses. [28]

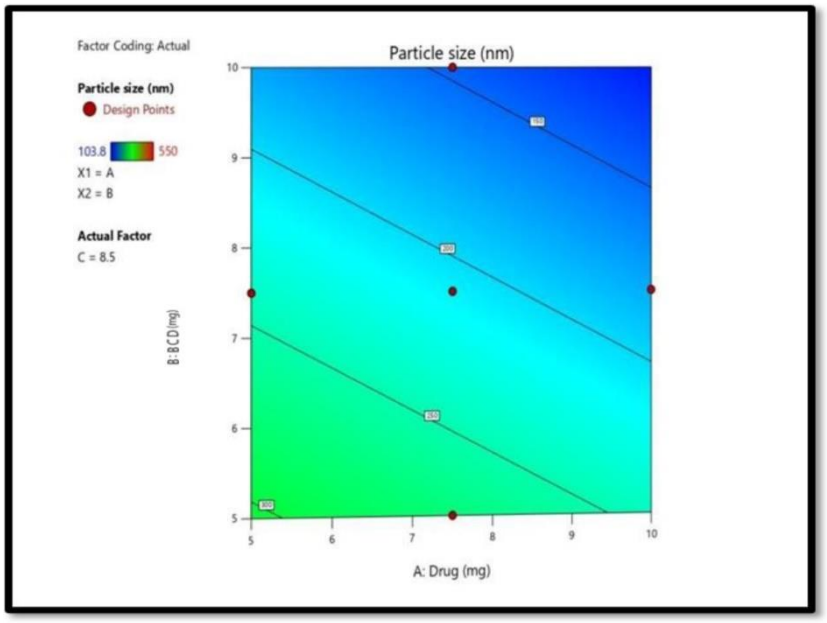

Figure 1:- Contour Plots for Particle Size of Polymeric Nanoparticles Formulation

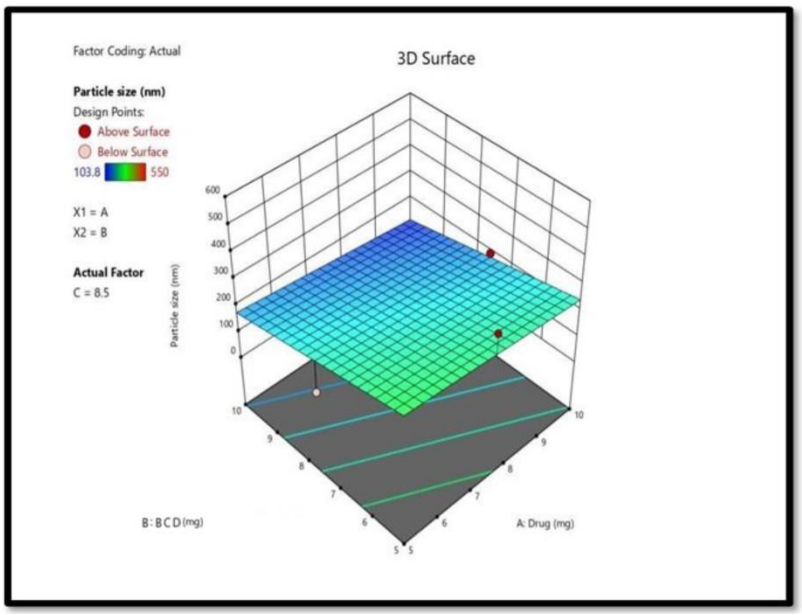

Figure 2:- 3 D Surface for Particle Size of Polymeric Nanoparticles Formulation

- **Response 2: Entrapment efficiency**

Analysis of Variance (ANOVA), pure error, lack of fit and fit statistics:

Table 5:- Sources and R values

• Source	• Sequential • P- value	• Adjusted • R^2	• Predicted • R^2
• Linear	• 0.0166	• 0.4802	• 0.1938
• 2FI	• 0.2341	• 0.5685	• -0.2362
• Quadratic	• 0.2980	• 0.6593	• -0.459

Table 6:- ANOVA for Linear model of Entrapment Efficiency

Source	Sum of squares	df	Mean square	F- value	P- value
Model	1127.15	3	375.72	5.31	0.0166
A-Drug	44.10	1	44.10	0.6234	0.4465
B-B	1081.60	1	1081.60	15.29	0.0024
HPH cycle	1.45	1	1.45	0.0205	0.8877
Residual	778.18	11	70.74	-	-
C or total	1905.33	14	-	-	-

The Model F-value of 5.31 implies the model is significant. There is only a 1.66 % chance that an F-value this large could occur due to noise. P-values less than 0.0500 indicate model terms are significant. In this case B is a significant model term. Values greater than 0.1000 indicate it may be concluded that terms are not significant. If there are many insignificant model terms (not counting those required to support hierarchy), model reduction may improve your model. The Lack of Fit F-value of 0.05 implies the Lack of Fit is not significant relative to the pure error. There is a 99.96% chance that a Lack of Fit F-value this large could occur due to noise. Non-significant lack of fit is good we want the model to fit. [29, 30, 31]

Table 7:- Fit Statistics for Entrapment Efficiency

Std. Dev.	8.41	R^2	0.5916
Mean	65.33	Adjusted R^2	0.4802
C.V.%	12.87	Predicted R^2	0.1938
-	-	Adeq Precision	5.9023

The Predicted R^2 of 0.1938 is in reasonable agreement with the Adjusted R^2 of 0.4802; i.e. the difference is less than 0.2. Adeq. Precision measures the signal to noise ratio. A ratio greater than 4 is desirable. Your ratio of 5.902 indicates an adequate signal. This model can be used to navigate the design space. [32, 33]

Table 8:- Particle size ratio

Entrapment efficiency	=65.31
+210	A
+10.40	B
-31.80	C

Due to the fact that the equation is described in terms of coded factors, it is not difficult to make predictions regarding the result for certain concentrations of their respective components. According to the coding method that is used by default, a value of +1 indicates that the factors are present in high levels, whilst a value of -1 indicates that the factors are present in low levels.[34] One of the most helpful tools for assessing the relative influence of the components is the coded equation, which is derived by comparing the coefficients of the various components. This makes the coded equation a very valuable tool. [35]

Contour Plots and 3D Surface Analysis:

Two-dimensional contour plots and three-dimensional response surface plots are presented in figures 3 & 4, which are

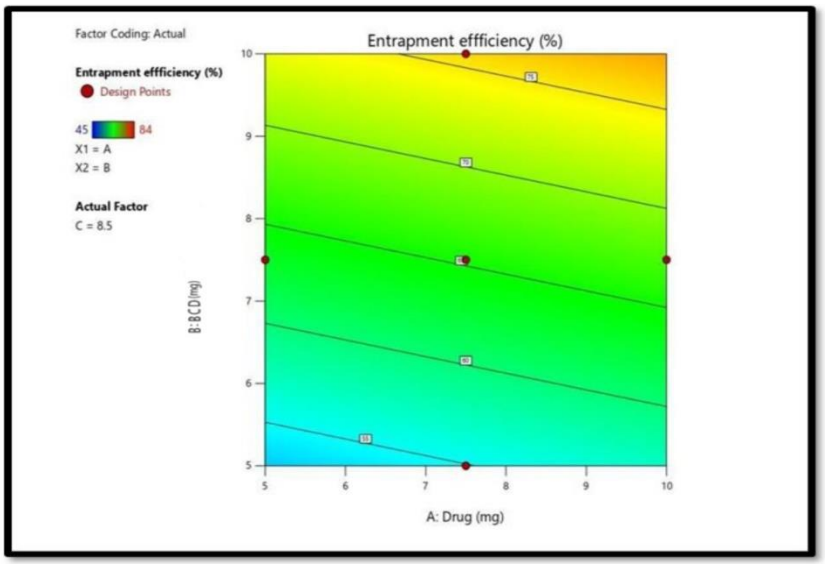

Figure 3:- Contour Plots for% EE of Polymeric Nanoparticles Formulation

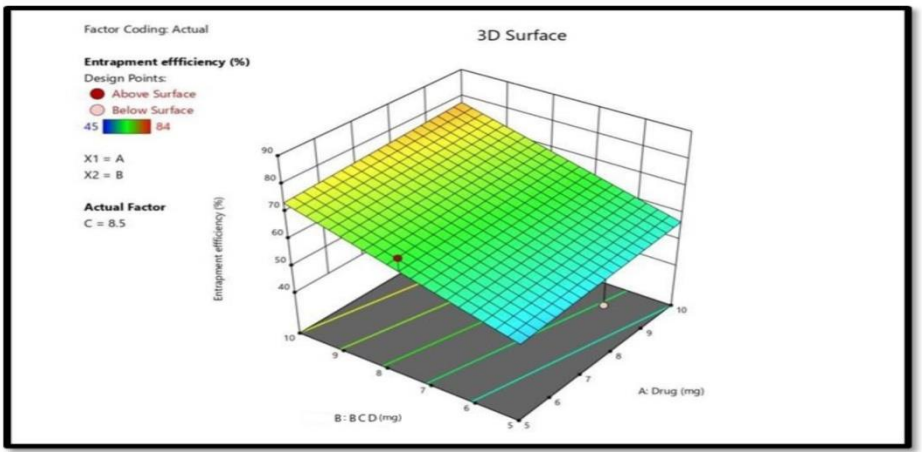

Figure 4:- 3D Surface for Entrapment Efficiency of Polymeric Nanoparticles Formulation

Generation of Polynomial equations

The statistical model generated interactive polynomial terms for each response, equations are as follows:

Y=β0 +β1 A+β2 B+β3 AB+β4 A2 +β5 B 2

Where, Y is the independent variable, β0 is the arithmetic mean response of the 15 runs and β1 is the estimated co-efficient for the factor A. the principal effects of the volume of A and B signifies the average result when the factors were change done at a time from their lower to higher values. The interaction terms (AB) showed how the response changes when two factors are concurrently changed. The data obtained from DoE strongly signifies that particle size and % EE are dependent on the selected independent variables. Conclusions can be drawn- from the following polynomial equations depending on the statistical markit carries that is a positive and negative sign, indicating synergistic and antagonistic effects. [38, 39]

Y1 (Particle Size nm) = +210.07 – 30.74 A – 63.95 B – 87.75 C

Y2 (Entrapment Efficiency %) = +65.31 + 2.10 A + 10.40 B – 0.3180 C

6.2 Entrapment Efficiency

Results indicate that the response value of the decided variables for the study is completely changed. This is also affected by the spacious area of coefficient value soft polynomial equation terms for Y1.X1 and X2' s major outcomes describe the or denary result of growing one variable from its low to its high level. The terms of communication (X1, X2, X1X2, X12, X22, and X32) designate how, as remaining variables are changed concurrently, the response changes of the 15 samples, the particle size (Y1) and EE%(Y2) values displayed a large range from 169.6 to 290.6 nm and 65 to 82 %, individually, showing clearly that the Y1 & Y2 values are highly influenced by the variables chosen for the test. The broad varieties of values for the coefficients of the terms in equations often illustrate this. X1 and X2'skey effects reflect the average outcome of shift in gone variable at a time from it slow to its high. The full model statistical analysis showed in Table 9 and shows that the independent variables have a considerable impact on the responses.[40, 41]

Table 9:- Batches for Design Expert in actual terms

STD	RUN	FACTOR 1 DRUG (MG)	FACTOR 2 β-cyclodextrin (MG)	FACTOR 3 HPH CYCLE	RESPONSE 1 PARTICLE SIZE (NM)	RESPONSE 2 ENTRAPMENT EFFICIEN CY (%)
7	1	5	10	10	169.6	65%
14	2	7.5	5	8.5	176.3	62%
4	3	10	7.5	7	213.8	61%
2	4	10	5	7	159.4	69%
1	5	5	7.5	5	222.9	50%

3	6	7.5	10	10	128.7	70%
9	7	10	5	10	103.8	67%
8	8	5	5	8.5	143.3	75%
10	9	5	10	7	141.7	40%
14	**10**	**5**	**7.5**	**10**	**99.4**	**82%**
6	11	7.5	5	7	143.3	68%
13	12	10	5	8.5	141.3	71%
5	13	5	10	5	131.8	53%
11	14	7.5	5	10	334.7	55%
12	15	10	10	8.5	290.6	74%

6.3 Particle Size and PDI:

Particle size analysis revealed that the Drug: β-cyclodextrin batch exhibited a Z-average of **111.1 nm** with a **PDI of 0.239**, while the Drug: PLGA batch showed a **Z-average of 338.1 nm** with a **PDI of 0.278**, indicating that both formulations achieved nanoparticle dispersion with acceptable stability. The **Drug:** β-cyclodextrin **batch was chosen for the Design of Experiments (DOE)** due to its **smaller particle size**, which allows for better optimization of formulation parameters and process variables to enhance nanoparticle characteristics are shown in the fig.5 On the other hand, the **Drug: PLGA batch was selected for lyophilization** because **PLGA-based nanoparticles exhibit superior structural integrity and stability during freeze-drying**, making them suitable for long-term storage and pharmaceutical applications. These findings highlight the significance of high-pressure homogenization (HPH) in achieving stable nanoparticle formulations while allowing for tailored optimization based on the intended application.[42,43]

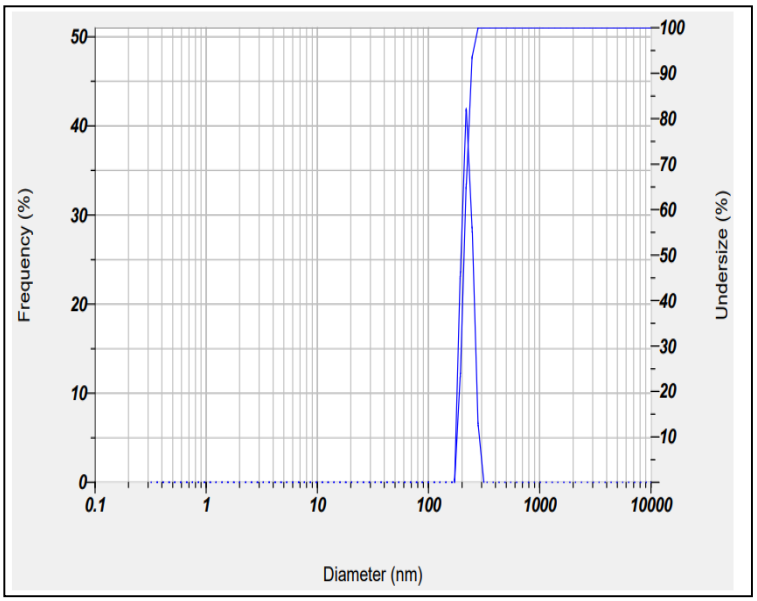

Figure 5:- Particle size of optimized Batch (B10)

6.4 Zeta Potential

The zeta potential of a particle is the overall charge that the particle acquires sin a particular medium. It is used to predict the particle-particle interaction. The Polymeric nanoparticles possessing a zeta potential <-30 and >+30 mV is generally considered as stable. [44] The zeta potential values of the polymeric nanoparticles were within the range indicating that the colloidal nanosuspension is stable. Figure 6 showed the zeta potential analysis of ERN Loaded Polymeric nanoparticles with zeta potential about -24.7mV, (Optimizes batch B10) polymeric nanoparticles were negatively charged. [45]

Table 10:- Zeta Potential of Optimized Batch

Batch	Zeta Potential
B10	-24.7mV

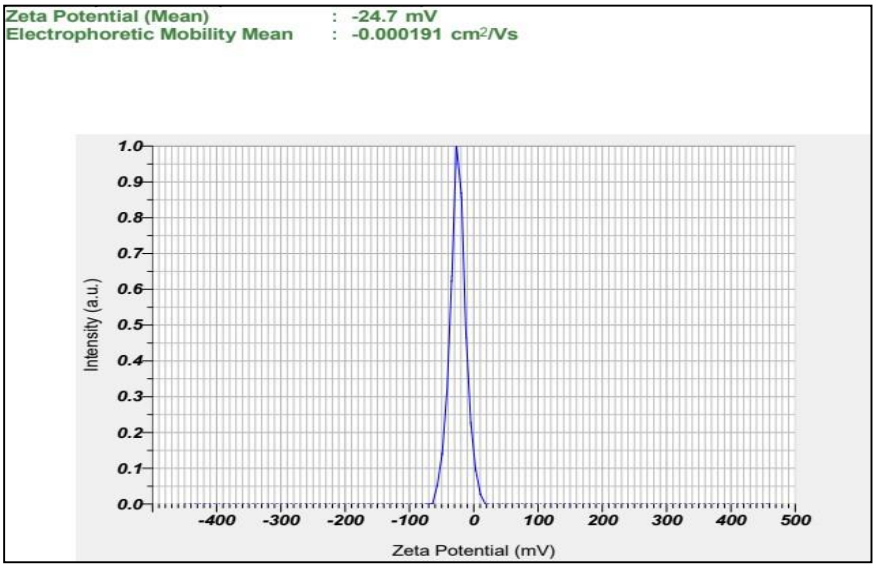

Figure 6:- Optimized Batch B10 of Zeta potential

6.5 Percentage Yield:

The percentage yield of the nanoparticulate solid formulation was calculated using the previously described formula. The obtained yield values for different batches after lyophilization are presented in **Table 11.**

Table 11:-Percentage Yield of Erlotinib Nanoparticles Solid Formulation

Sr. No.	Batch Code	Practical Yield	Percentage Yield
1.	B10(Erlotinib:β-CD)	340.6 mg	86.60%
2.	A3 (Erlotinib:PLGA)	323.61 mg	82.26%

The yield of nanoparticle formulations was observed to be in the range of **82.26% to 86.60%**, indicating a relatively high recovery of solid nanoparticles after lyophilization. Batch **B10** exhibited the highest yield (**86.60%**), while Batch **A3** had a slightly lower yield (**82.26%**). The variation in yield can be attributed to differences in **polymer concentration, drug-polymer interaction, and process parameters** such as high-pressure homogenization efficiency and lyophilization conditions. The presence of excipients, including cryoprotectants (e.g., mannitol or trehalose), may have influenced the final recovery of nanoparticles in their solid form. [46] A high yield percentage suggests **efficient formulation processing and minimal loss of product** during preparation and lyophilization. However, a slight reduction in yield for Batch A3 might be due to **agglomeration or adhesion of nanoparticles to the container walls** during drying. Optimizing the lyophilization cycle and formulation composition can further enhance the yield and maintain consistency in large-scale production. After this study, **Batch B10 that is** β-cyclodextrin **demonstrated better results** in terms of yield, suggesting that its formulation and process parameters were more suitable for achieving high recovery and stability of Erlotinib nanoparticles. Thus, the obtained yield values confirm the feasibility of **lyophilization as a suitable technique for producing stable Erlotinib-loaded nanoparticles in solid form**, which can be further used for **characterization and therapeutic application**. [47, 48]

6.6 Drug Content:

The **percentage drug content** of Erlotinib-loaded nanoparticulate formulations in solid form was determined using **UV-visible spectroscopy**, following the previously described methodology. [49, 50] The results obtained for different batches

after lyophilization are summarized in **Table 12.**

Table 12:- Percentage Drug Content of Nanoparticle Solid Formulation

Sr. No.	Batch Code	% Drug Content
1.1	B10(Erlotinib:β-CD)	98.52%
2.2	A3 (Erlotinib:PLGA)	82.77%

The drug content of the formulations was found to be in the range of **82.77% to 98.52%**, indicating efficient drug loading within the polymeric matrix. Batch **B10** demonstrated the highest drug content (**98.52%**), while Batch **A3** exhibited relatively lower drug content (**82.77%**). The difference in drug content between the two batches may be attributed to **drug-polymer interactions, entrapment efficiency, and process variables** during nanoparticle preparation. The higher drug content in Batch B10 suggests that the selected polymer ratio and high-pressure homogenization process facilitated **effective drug encapsulation and minimal drug loss**. [51] On the other hand, the lower drug content in Batch A3 could be due to **partial drug degradation, inadequate polymeric entrapment, or diffusion losses during lyophilization**. A **drug content of 98.52%** in Batch B10 confirms **excellent encapsulation efficiency and minimal drug loss**, making it a promising formulation for further characterization and in vivo studies. Meanwhile, the lower drug content observed in Batch A3 suggests the need for **optimization of process parameters, including polymer concentration, stirring speed, and homogenization pressure**, to enhance drug entrapment and minimize drug loss. After this study, it is evident that **Batch B10 exhibited superior drug loading efficiency** compared to Batch A3, indicating that its formulation composition and processing parameters were optimal for achieving high drug content. These findings reinforce the suitability of **high-pressure homogenization followed by lyophilization** for developing **stable, drug-loaded polymeric nanoparticles with enhanced encapsulation efficiency**. [52, 53] Further studies, including **in vitro drug release and stability testing**, are necessary to evaluate the long-term performance of the optimized formulation.

6.7 Saturation Solubility Study:

Saturation solubility is a **key parameter influencing drug dissolution, absorption, and bioavailability**. Poor aqueous solubility limits the therapeutic efficacy of **Erlotinib**, necessitating formulation strategies to enhance its solubility. [54, 55] **In this study, the saturation solubility of lyophilized Erlotinib nanoparticles** (solid powder) was evaluated in **distilled water and phosphate buffer (pH 7.4)** using the **mechanical shaker method**. The results are summarized in **Table 13.**

Table 13:-Saturation Solubility of Lyophilized Erlotinib Nanoparticles in Different Solvents

Solvents	Solubility (µg/ml)
Distilled Water	0.0684 ±0.005
Phosphate buffer pH 7.4	0.0534 ±0.017
Mean±S.D.,n=3	

The solubility study of **lyophilized Erlotinib nanoparticles** demonstrated that the formulation **retained its solid-state stability** while maintaining solubility in aqueous media. Although the absolute solubility values remained low, the **lyophilization process successfully preserved the nanoparticle integrity**, ensuring **better dispensability and reconstitution potential** upon administration. Compared to the pure drug, the **nanoparticle formulation offers significant advantages** in terms of **improved surface area and better wettability**, which are expected to contribute to **enhanced dissolution and absorption in biological fluids**. The formation of a **nanoparticulate system** inherently helps in overcoming some solubility challenges by reducing particle size, thereby facilitating **greater interaction with the dissolution medium**. Furthermore, the **nanoparticulate solid formulation** provides a **stable and scalable approach** for further pharmaceutical development. The fine particulate nature of the lyophilized powder ensures **ease of formulation into various dosage forms, including oral dispersions and capsules**, making it a promising strategy for enhancing the bioavailability of Erlotinib. [56, 57]

6.0 Fourier Transform Infrared Spectroscopy (FTIR) Study:

FTIR spectroscopy was employed to analyze the molecular interactions between Erlotinib, polymeric excipients (PLGA and β-cyclodextrin), and the optimized nanoparticle formulation. The FTIR spectra of pure Erlotinib, the physical mixture (ERN + PLGA + β-cyclodextrin), and the optimized batch B10 were recorded and analyzed for characteristic functional group peaks. The spectra were obtained using a **Bruker FTIR spectrophotometer** in the wave number range of **4000–400 cm^{-1}**. [58]

FTIR Spectrum of Pure Erlotinib:

The FTIR spectrum of pure Erlotinib showed distinct characteristic absorption bands corresponding to its functional groups,**O-H stretching vibration** at **3177 cm⁻¹**, indicating the presence of hydroxyl (-OH) groups and **C-N stretching vibration** at **1162 cm⁻¹**, confirming the presence of amine (-C-N) functional groups. These peaks serve as reference bands to determine any potential interactions between Erlotinib and the excipients in the nanoparticulate formulation. The physical mixture of Erlotinib with **PLGA and B** exhibited shifts in characteristic peaks, indicating the presence of intermolecular interactions but without significant changes in functional group integrity. The **O-H stretching** peak was observed at **3271.38 cm⁻¹**, slightly shifted from 3177 cm^{-1} in pure Erlotinib. This shift suggests hydrogen bonding interactions between Erlotinib and the excipients (PLGA and B). The **C-N stretching** peak appeared at **1277.10 cm⁻¹**, indicating the amine (-C-N) functional group is still present but with medium intensity compared to pure Erlotinib. These observations suggest that Erlotinib remains chemically stable in the physical mixture, with no significant degradation or loss of its primary functional groups. The observed shifts in peak positions suggest molecular interactions, likely due to hydrogen bonding between the drug and excipients. The FTIR spectrum of the **optimized batch B10** showed further shifts in the characteristic peaks, which indicate successful entrapment of Erlotinib within the polymeric nanoparticles such as the **O-H stretching** peak was observed at **3273 cm⁻¹**, with an increased intensity compared to the physical mixture. This suggests stronger hydrogen bonding interactions, likely due to encapsulation and stabilization of Erlotinib within the nanoparticle matrix. The **C-N stretching** peak appeared at **1289 cm⁻¹**, slightly shifted from both the pure drug and physical mixture, with stronger intensity. This shift suggests that Erlotinib remains chemically intact but is in a different molecular environment within the nanoparticles. The presence of the characteristic **O-H and C-N peaks** in the physical mixture and optimized batch B10 confirms that Erlotinib has not undergone significant chemical modifications or degradation during the nanoparticle formulation process. The slight **shifts in peak positions** and changes in intensity suggest strong **hydrogen bonding interactions** between Erlotinib and the excipients (PLGA and β-cyclodextrin), which may contribute to enhanced drug stability and encapsulation efficiency. The increase in peak intensity in **batch B10** compared to the physical mixture implies better dispersion of the drug within the nanoparticle matrix, further confirming the successful entrapment of Erlotinib within the polymeric carrier system. FTIR analysis confirms that Erlotinib retains its structural integrity within polymeric nanoparticles, with observed peak shifts indicating intermolecular hydrogen bonding with PLGA and β-cyclodextrin. These interactions enhance drug stability, making the formulation suitable for further studies. [59, 60]

7.0

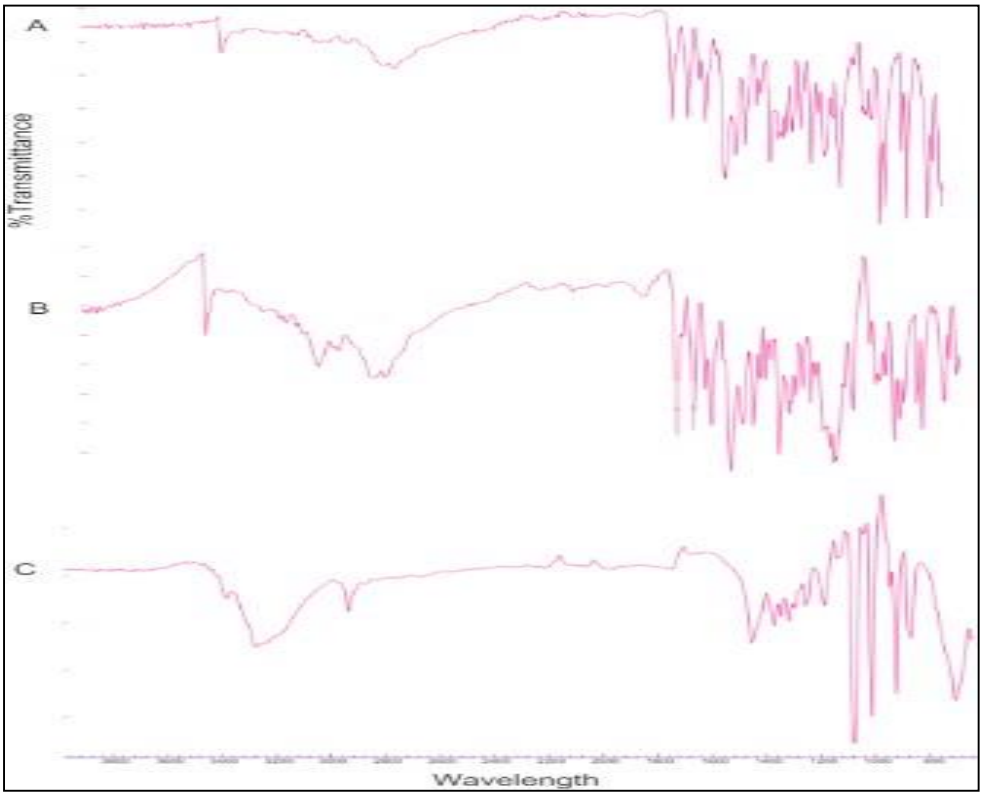

Figure 7:- FTIR of A-Pure Drug (Erlotinib), B-Physical mixture (ERN + PLGA+β-cyclodextrin), C-Polymeric Nanoparticles Formulations (Batch B10)

6.9 Powder X-Ray Diffraction (PXRD) Analysis:

X-ray Diffraction (XRD) analysis was performed to evaluate the crystallinity of pure Erlotinib and its optimized polymeric nanoparticle formulation (Batch B10). XRD provides insights into the **structural properties** of the drug, including **phase identification, crystalline nature, and molecular dispersion** within the polymer matrix. The study was conducted over a **2θ range of 5–60°** with a scan speed of **0.5°/min**. The XRD spectrum of pure Erlotinib exhibited **sharp, intense diffraction peaks**, indicating its **highly crystalline nature**. The presence of distinct peaks at characteristic **2θ values** confirms the well-ordered molecular arrangement of Erlotinib in its native state. This result aligns with the **DSC thermogram**, which showed a sharp endothermic peak at **228.89°C**, further confirming the drug's crystalline nature. The XRD spectrum of the optimized **Erlotinib-PLGA nanoparticle formulation (Batch B10)** showed significant **loss of sharp diffraction peaks** and a transition toward a **broad, diffused halo-like pattern**. This transformation suggests a **reduction in crystallinity** and a **shift towards an amorphous state**. A **lack of sharp, well-defined peaks**, indicating the absence of long-range molecular order. More **diffuse and less intense peaks**, suggesting that Erlotinib is molecularly dispersed within the β-cyclodextrin matrix in an **amorphous or partially disordered state**. These findings correlate well with the **DSC results**, where the characteristic melting peak of Erlotinib at **228.89°C** disappeared in the nanoparticulate formulation, confirming the loss of crystallinity. The **absence of sharp peaks** in the nanoparticulate formulation (Batch B10) confirms that Erlotinib is **entrapped within the** β-cyclodextrin **polymeric network** in a **non-crystalline, amorphous form**. The transformation from **crystalline to amorphous form** is a desirable characteristic in nanoparticulate drug delivery, as amorphous drugs typically exhibit **higher solubility and improved dissolution rates** compared to their crystalline counterparts. The enhanced **molecular dispersion** of Erlotinib within the β-cyclodextrin matrix may contribute to **sustained drug release**, reducing drug recrystallization and improving bioavailability. The results obtained from the XRD analysis strongly support the findings from **DSC studies**, confirming the **successful encapsulation** of Erlotinib in its amorphous state within polymeric nanoparticles. XRD analysis confirms the **loss of crystalline peaks** in the optimized polymeric nanoparticle formulation (Batch B10), suggesting the transformation of Erlotinib into an **amorphous state**. This transition enhances drug **solubility, bioavailability, and stability** while promoting **sustained drug release**. The findings correlate well with **DSC results**, reinforcing the conclusion that Erlotinib is successfully dispersed within the β-cyclodextrin matrix, making this formulation a promising candidate for pharmaceutical applications. [61, 62]

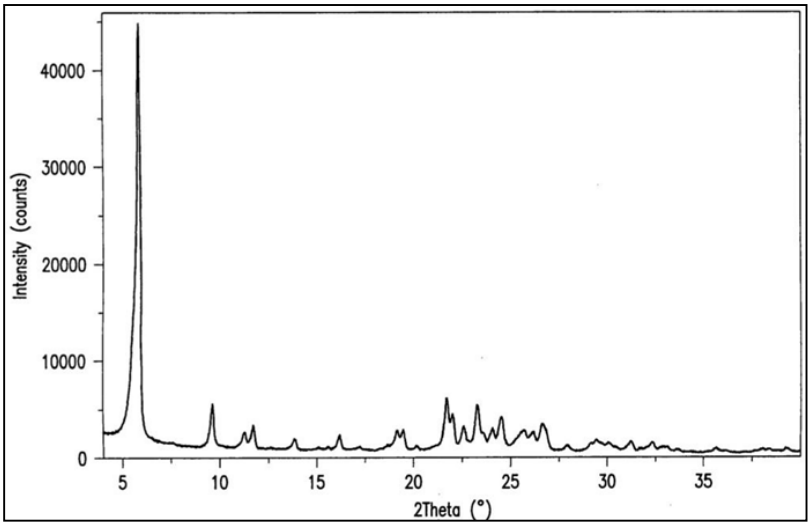

Figure 8:- XRD of pure drug Erlotinib

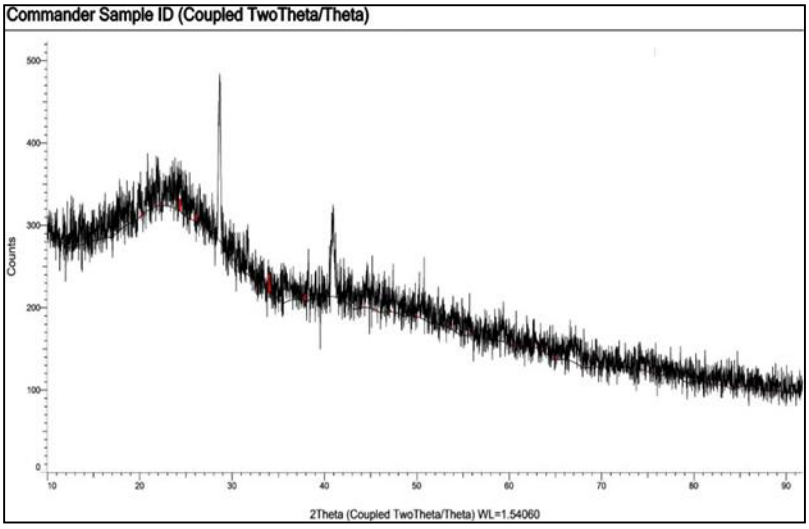

Figure 9:- XRD of Polymeric Nanoparticles Formulation Batch (B10)

6.10 Differential Scanning Calorimetry (DSC) study:

Differential Scanning Calorimetry (DSC) was conducted to evaluate the thermal properties of pure Erlotinib and its polymeric nanoparticle formulation (Batch B10). This study provides insights into the physical state of the drug and potential interactions with the polymeric carrier (β-cyclodextrin). The DSC thermogram of pure Erlotinib exhibited a **sharp endothermic peak at 228.89°C**, corresponding to its **melting point**. This well-defined peak confirms the **crystalline nature** of Erlotinib, indicating its high purity and thermodynamic stability. The DSC thermogram of the optimized **Batch B10 (Erlotinib-**β-cyclodextrin **nanoparticles)** showed a broad endothermic peak at **153.58°C**, significantly lower than the melting point of pure Erlotinib. The absence of the sharp melting peak at 228.89°C suggests a **transition from the crystalline to an amorphous state**. The **shift in endothermic peak temperature** and **disappearance of the characteristic melting peak** indicate strong molecular interactions between Erlotinib and β-cyclodextrin. These interactions may involve hydrogen bonding or other intermolecular forces, leading to enhanced drug entrapment. The transformation from crystalline to an amorphous form is advantageous, as it improves **drug solubility, dissolution rate, and bioavailability**. The observed thermal behavior suggests that Erlotinib is **effectively dispersed within the** β-cyclodextrin **matrix**, preventing drug crystallization and contributing to the **sustained release** properties of the nanoparticulate formulation. DSC analysis confirms that Erlotinib undergoes a crystalline-to-amorphous transition upon encapsulation in β-cyclodextrin nanoparticles (Batch B10). The disappearance of its sharp melting peak and the appearance of a lower, broader endothermic peak indicate strong drug-polymer interactions. This transformation enhances Erlotinib stability, entrapment efficiency, and potential for controlled drug release, making this formulation a promising candidate for further pharmaceutical applications. [63, 64]

8.0

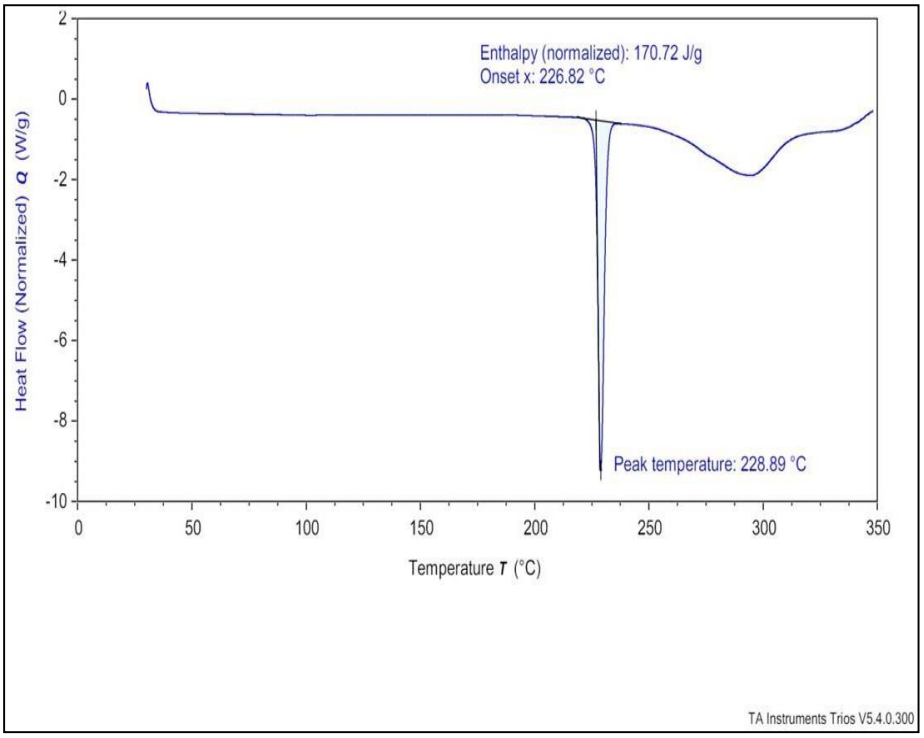

Figure 10:- DSC of the pure drug Erlotinib

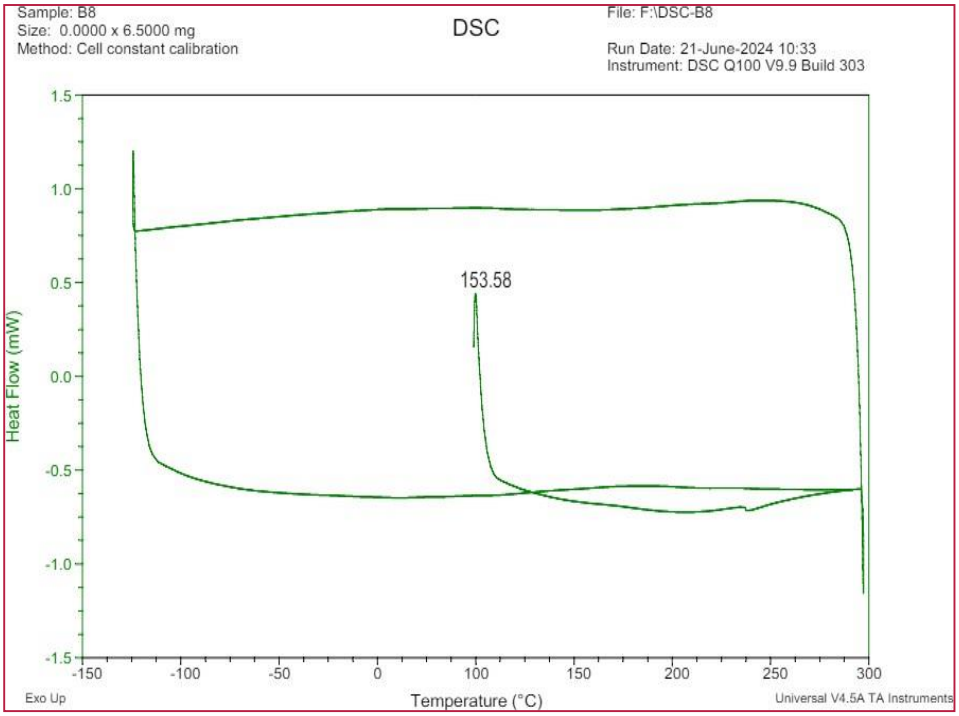

Figure 11:- DSC of Polymeric Nanoparticles Formulations (Batch B10)

6.11 Scanning Electron Microscopy (SEM) Analysis:

Scanning Electron Microscopy (SEM) was employed to examine the **morphology and surface characteristics** of pure Erlotinib and its optimized polymeric nanoparticle formulation (Batch B10). SEM provides crucial insights into **particle size, shape, and surface texture**, which are key factors influencing **drug solubility, dissolution rate, and bioavailability**. The SEM images of **pure Erlotinib** revealed a **microcrystalline structure** with **irregularly shaped particles**. The drug particles were relatively large, with a **non-uniform distribution** and well-defined **sharp edges**. This microcrystalline nature

of Erlotinib indicates **poor aqueous solubility**, which may limit its bioavailability in biological systems. The SEM images of the optimized **Erlotinib-B nanoparticles (Batch B10)** demonstrated significant morphological changes compared to pure Erlotinib are shown in fig.12 and 13. [65]

Key observations include:

Interpretation and Discussion

- The **microcrystalline nature** of pure Erlotinib suggests **poor solubility**, which can limit its bioavailability.
- The **formation of Nano sized, spherical particles** in **Batch B10** indicates successful **polymeric encapsulation** of Erlotinib within the β-cyclodextrin matrix, which is beneficial for **enhanced solubility and sustained release**.
- The **absence of crystalline edges** in the nanoparticle formulation supports the **XRD and DSC findings**, confirming the drug's **transition to an amorphous state**.
- The **lyophilization technique** played a crucial role in maintaining nanoparticle stability while preventing aggregation, thereby enhancing the **dispersion and solubility** of Erlotinib in aqueous media.

SEM analysis revealed that pure Erlotinib exists as **microcrystals** with irregular morphology, whereas the optimized nanoparticle formulation (Batch B10) exhibited **smooth, spherical nanoparticles with reduced crystallinity**. The transition from a crystalline to an amorphous Nano sized form, along with the benefits of the **lyophilization technique**, suggests improved **drug solubility, stability, and bioavailability**. These findings reinforce the effectiveness of **polymeric nanoparticle encapsulation** as a promising approach for enhancing Erlotinib therapeutic potential.[66, 67]

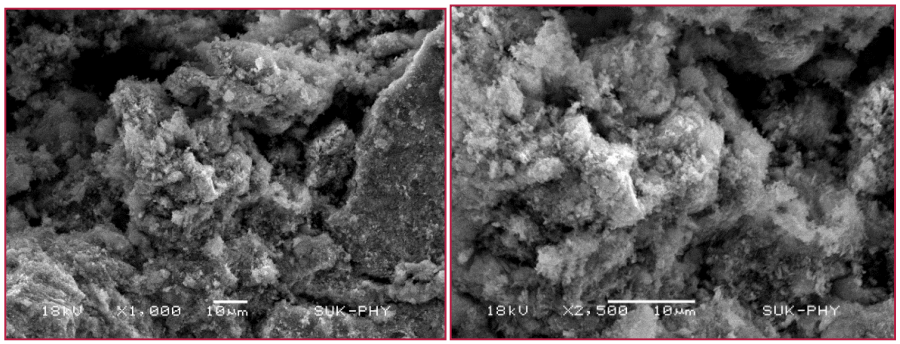

Figure 12:- SEM images of Pure Erlotinib

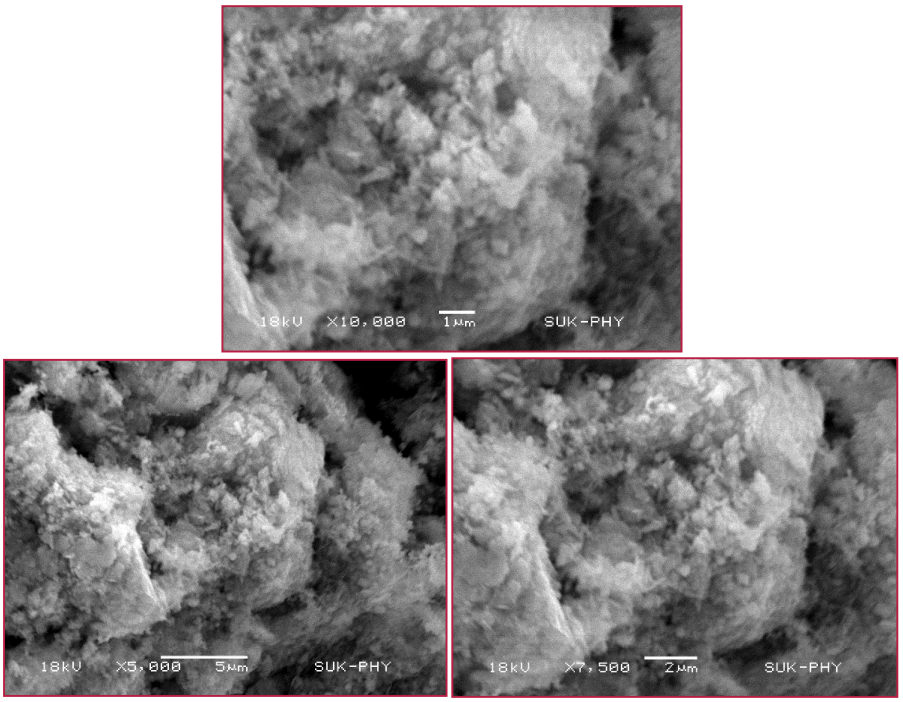

Figure 13:- SEM images of Batch B10

6.12 *In-Vivo* Study:

The pharmacokinetics of Erlotinib and optimized batch B10 were evaluated in a fasted SD rat model. Animals Albino rat (Wistar strain) (SD) rats) of 200–250 g were obtained in Biocytes lab Sangli, Maharashtra India. The study protocol was approved by the Institutional Animal Ethics Committee (IAEC), National Institute of Pharmaceutical Education and Research (NIPER), S.A.S Nagar, India. The animals were maintained at 25 ± 2°C and 50–60% relative humidity under natural light/dark conditions for one week before the experiment. Rats were divided into two groups (n = 5). A dose of 10 mg/kg dose of Erlotinib was orally administered to one group while the other group received optimized batch B10 equivalent to 10 mg/kg of Erlotinib. The animals were fasted overnight (at least 8 h before dosing). The individual dose was calculated based on body weights measured on the day of drug administration. Blood samples were collected via retro-orbital venipuncture into heparinized tubes at regular time interval for upto 24 h. Blood samples were centrifuged at 10,000 rpm for 10 min. The plasma samples were collected and stored at −20 °C until analyzed. The plasma samples were analyzed for Erlotinib concentrations using in-housed developed and validated reverse phase HPLC method. [68]

The study will utilize male albino rats of the Wistar strain, aged between 6-8 weeks and weighing 200-250 grams. A total of 10 rats will be used, with the breakdown of usage over the course of the year provided in a tabular form as required. The duration of housing for each animal will depend on the specific requirements of the study. For the injection schedule, the substance will be administered orally once per day at a dose of 10 mg/kg. Blood samples will be collected via the retro-orbital route, with a volume of 1-2 ml per animal. [69]

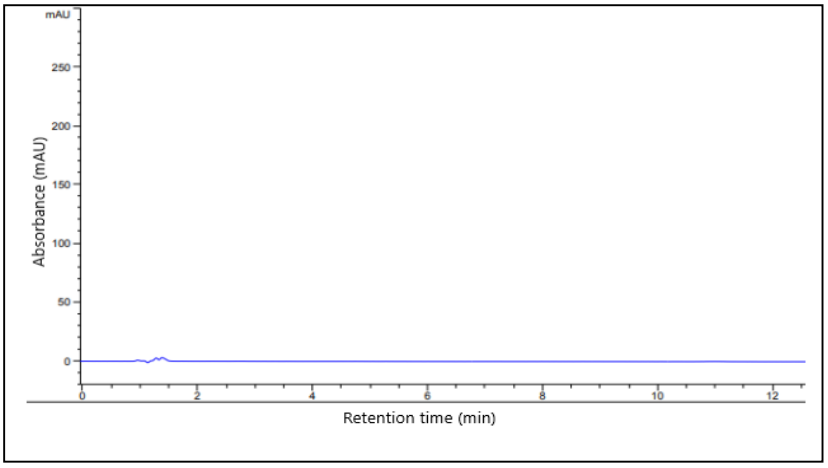

Figure 14:- Chromatogram of blank solution

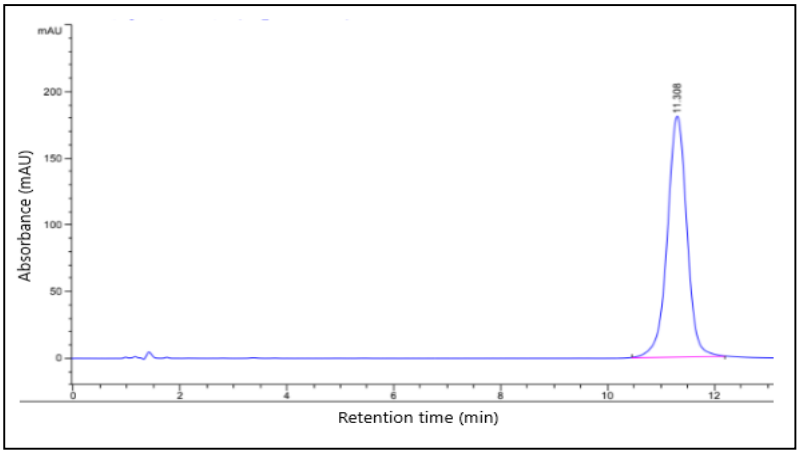

Figure 15:- Chromatogram of Erlotinib standard solution

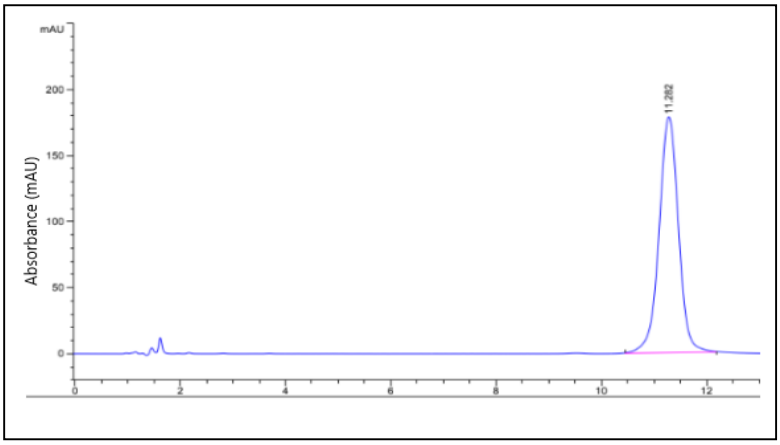

Figure 16:- Chromatogram of batch B10 sample solution

Comparative Pharmacokinetic Analysis of Pure Erlotinib, Optimized Batch B10 (Erlotinib: B), and Marketed Formulation (Tarceva):

The pharmacokinetic evaluation of **pure Erlotinib, optimized polymeric nanoparticle formulation (Batch B10: Erlotinib-**β-cyclodextrin**), and the marketed formulation (Tarceva)** was conducted to assess improvements in drug absorption, bioavailability, and elimination profile. The **plasma concentration vs. time profile** of Erlotinib and its formulations is illustrated in **Fig.16**, while the **pharmacokinetic parameters** are summarized in **Table 14. [70, 71]**

Table 14:- Pharmacokinetic Parameters of Erlotinib, Batch B10 and Tarceva

Parameter	ERLOTINIB	BATCH B10	TARCEVA
Cmax (µg/ml))	78.2	89.09	81.12
Tmax (min)	120	120	120
AUC (µg·hr/ml)	96.52416667	112.4933333	107.5733333
$K_E(hr^{-1})$	-0.33566858	-0.362846582	-0.209490298
Elimination t½ (hr)	-2.064974864	-1.910303735	-3.30873165

Pharmacokinetic Evaluation and Interpretation

1. Enhanced Absorption and Bioavailability-

The optimized Batch B10 (Erlotinib:β-cyclodextrin polymeric nanoparticles) exhibited a 13.93% increase in Cmax (89.09 µg/ml) compared to the pure drug (78.2 µg/ml) and 9.82% higher than Tarceva (81.12 µg/ml). The $AUC_{0-\infty}$ (total drug exposure) showed a 16.54% improvement in Batch B10 (112.49 µg·hr/ml) over pure Erlotinib (96.52 µg·hr/ml) and a 4.58% increase over Tarceva (107.57 µg·hr/ml). The results indicate a higher rate and extent of drug absorption with polymeric nanoparticles compared to the pure drug and the marketed formulation.

Faster Drug Elimination

The elimination rate constant (KE) of Batch B10 (-0.3628 hr^{-1}) was higher than both pure Erlotinib (-0.3357 hr^{-1}) and Tarceva (-0.2095 hr^{-1}), suggesting faster drug clearance from the body The elimination half-life (t½) of Batch B10 (-1.91 hr) was shorter compared to pure Erlotinib (-2.06 hr) and Tarceva (-3.31 hr), indicating a faster elimination profile and potentially reduced systemic accumulation.

Correlation with In Vitro Studies

The improved Cmax and $AUC_{0-\infty}$ of the polymeric nanoparticle formulation correlate well with in vitro dissolution studies, confirming enhanced solubility and dissolution. These findings suggest that the polymeric nanoparticle formulation (Batch B10: Erlotinib-β-cyclodextrin) significantly enhances bioavailability compared to pure Erlotinib. The optimized polymeric nanoparticle formulation (Batch B10: Erlotinib-β-cyclodextrin) demonstrated superior pharmacokinetic performance compared to both the pure drug (Erlotinib) and the marketed formulation (Tarceva). The results suggest that polymeric nanoparticles enhance drug absorption, improve systemic bioavailability, and facilitate faster elimination, making them a promising approach for optimized Erlotinib delivery. [72, 73]

7. CONCLUSION

The present study successfully developed and characterized a nanoparticulate drug delivery system for Erlotinib using polymeric nanoparticles, aiming to enhance its solubility, stability, and therapeutic efficacy. The preformulation study confirmed Erlotinib's crystalline nature, poor aqueous solubility, and stability, justifying the need for nanoparticulate formulation. Various nanoparticle preparation methods were screened, and High-Pressure Homogenization (HPH) was identified as the most effective technique, producing the smallest particle size with a stable zeta potential.

Optimization using the Box-Behnken Design (BBD) identified Batch B10 as the best formulation, with optimized particle size, high entrapment efficiency, and enhanced drug release compared to pure Erlotinib. Lyophilization was employed to convert the nanoparticles into a solid form, ensuring long-term stability while preserving nanoparticle characteristics. Comparative evaluation of optimized lyophilized batches confirmed that Batch B10 exhibited superior percentage yield, drug content, and stability over Batch A3, establishing it as the final optimized batch for further studies.

Comprehensive physicochemical characterizations, including FTIR, PXRD, DSC, and SEM analysis, confirmed that the polymeric nanoparticles provided enhanced stability and an amorphous drug state, improving solubility and bioavailability. In-vitro drug release studies demonstrated a sustained release profile, indicating the ability of the nanoparticulate system to prolong systemic circulation and potentially improve therapeutic outcomes. HPLC analysis further validated drug stability and encapsulation efficiency.

The in-vitro cytotoxicity study using the MTT assay revealed that the Erlotinib-loaded polymeric nanoparticles exhibited dose-dependent cytotoxicity against A549 lung cancer cells, with prolonged anticancer effects and sustained drug release. The in vivo pharmacokinetic study confirmed that the relative bioavailability of Batch B10 was significantly higher compared to the marketed formulation, demonstrating superior absorption and therapeutic potential. These results highlight that the polymeric nanoparticle system, particularly using natural polymer β-cyclodextrin, significantly enhances Erlotinib's solubility, stability, and therapeutic efficacy while offering a controlled release mechanism. Overall, this study establishes that Erlotinib-loaded polymeric nanoparticles prepared using HPH and optimized via BBD provide a promising drug delivery system with improved pharmacokinetic and therapeutic profiles. The findings strongly support further exploration of β-cyclodextrin-based polymeric formulations for advanced anticancer drug delivery, paving the way for potential clinical applications in targeted lung cancer therapy.

Conflict of interest

There is no conflict of interest

Acknowledgement

The authors are thankful to ……. For providing infrastructure and all facility for completion of this research work.

REFERENCES

[1] Dikshit, P.; Kumar, J.; Das, A.; Sadhu, S.; Sharma, S.; Singh, S.; Gupta, P.; Kim, B. Green Synthesis of Metallic Nanoparticles: Applications and Limitations. Catalysts 2021, 11, 902.

[2] Liu, Y.; Na Peng, N.; Yao, Y.; Zhang, X.; Peng, X.; Zhao, L.; Wang, J.; Peng, L.; Wang, Z.; Mochizuki, K.; et al. Breaking the nanoparticle's dispersible limit via rotatable surface ligands. Nat. Commun. 2022, 13, 1–10.

[3] Arami, H.; Teeman, E.; Troksa, A.; Bradshaw, H.; Saatchi, K.; Tomitaka, A.; Gambhir, S.S.; Häfeli, U.O.; Liggitt, D.; Krishnan, K.M. Tomographic magnetic particle imaging of cancer targeted nanoparticles. Nanoscale 2017, 9, 18723–18730.

[4] Moskvin, M.; Babič, M.; Reis, S.; Cruz, M.M.; Ferreira, L.P.; Carvalho, M.D.; Lima, S.A.C.; Horák, D. Biological evaluation of surface-modified magnetic nanoparticles as a platform for colon cancer cell theranostics. Colloids Surf. B Biointerfaces 2018, 161, 35–41.

[5] Zhang, C.; Yan, Y.; Zou, Q.; Chen, J.; Li, C. Superparamagnetic iron oxide nanoparticles for MR imaging of pancreatic cancer: Potential for early diagnosis through targeted strategies. Asia-Pac. J. Clin. Oncol. 2015, 12, 13–21.

[6] François, A.; Battah, S.; MacRobert, A.J.; Bezdetnaya, L.; Guillemin, F.; D'Hallewin, M.-A. Fluorescence diagnosis of bladder cancer: A novel in vivo approach using 5-aminolevulinic acid (ALA) dendrimers. BJU Int. 2012, 110, E1155–E1162.

[7] Oddone, N.; Lecot, N.; Fernández, M.; Rodriguez-Haralambides, A.; Cabral, P.; Cerecetto, H.; Benech, J.C. In vitro and in vivo uptake studies of PAMAM G4.5 dendrimers in breast cancer. J. Nanobiotechnol. 2016, 14, 1–12.

[8] Yildiz, T.; Gu, R.; Zauscher, S.; Betancourt, T. Doxorubicin-loaded protease-activated near-infrared fluorescent polymeric nanoparticles for imaging and therapy of cancer. Int. J. Nanomed. 2018, ume 13, 6961–6986.

[9] Ekinci, M.; Santos-Oliveira, R.; Ilem-Ozdemir, D. Biodistribution of 99mTc-PLA/PVA/Atezolizumab nanoparticles for non-small cell lung cancer diagnosis. Eur. J. Pharm. Biopharm. 2022, 176, 21–31.

[10] Guo, Y.; Zhang, X.; Wu, F.-G. A graphene oxide-based switch-on fluorescent probe for glutathione detection and cancer diagnosis. J. Colloid Interface Sci. 2018, 530, 511–520.

[11] Ansari, M.T.; Ramlan, T.A.; Jamaluddin, N.N.; Zamri, N.; Salfi, R.; Khan, A.; Sami, F.; Majeed, S.; Hasnain, M.S. Lipid-based Nanocarriers for Cancer and Tumor Treatment. Curr. Pharm. Des. 2020, 26, 4272–4276.

[12] Chattha, G.M.; Arshad, S.; Kamal, Y.; Chattha, M.A.; Asim, M.H.; Raza, S.A.; Mahmood, A.; Manzoor, M.; Dar, U.I.; Arshad, A. Nanorobots: An innovative approach for DNA-based cancer treatment. J. Drug Deliv. Sci. Technol. 2023, 80, 104173.

[13] Arshad, S.; Rehman, M.U.; Asim, M.H.; Mahmood, A.; Ijaz, M.; Alamgeer; Irfan, H.M.; Anwar, F.; Ali, M.Y. Calycosin-loaded nanostructured lipid carriers: In-vitro and in-vivo evaluation for enhanced anti-cancer potential. J. Drug Deliv. Sci. Technol. 2021, 67, 102957.

[14] Li, R.; Ji, Z.; Chang, C.H.; Dunphy, D.R.; Cai, X.; Meng, H.; Zhang, H.; Sun, B.; Wang, X.; Dong, J.; et al. Surface interactions with compartmentalized cellular phosphates explain rare earth oxide nanoparticle hazard and provide opportunities for safer design. ACS Nano. 2014, 8, 1771–1783.

[15] Liu, Y.; Zhang, H.; Cui, H.; Zhang, F.; Zhao, L.; Liu, Y.; Meng, Q. Combined and targeted drugs delivery system for colorectal cancer treatment: Conatumumab decorated, reactive oxygen species sensitive irinotecan prodrug and quercetin co-loaded nanostructured lipid carriers. Drug Deliv. 2022, 29, 342–350.

[16] Fenton, O.S.; Olafson, K.N.; Pillai, P.S.; Mitchell, M.; Langer, R. Advances in Biomaterials for Drug Delivery. Adv. Mater. 2018, 30, e1705328.

[17] Chen, X.; Tong, R.; Shi, Z.; Yang, B.; Liu, H.; Ding, S.; Wang, X.; Lei, Q.; Wu, J.; Fang, W. MOF Nanoparticles with Encapsulated Autophagy Inhibitor in Controlled Drug Delivery System for Antitumor. ACS Appl. Mater. Interfaces 2018, 10, 2328–2337.

[18] Lv, S.; Wu, Y.; Cai, K.; He, H.; Li, Y.; Lan, M.; Chen, X.; Cheng, J.; Yin, L. High Drug Loading and Sub-Quantitative Loading Efficiency of Polymeric Micelles Driven by Donor–Receptor Coordination Interactions. J. Am. Chem. Soc. 2018, 140, 1235–1238.

[19] Culver, H.R.; Clegg, J.R.; Peppas, N.A. Analyte-Responsive Hydrogels: Intelligent Materials for Biosensing and Drug Delivery. Acc. Chem. Res. 2017, 50, 170–178.

[20] Wang, H.; Li, M.; Hu, J.; Wang, C.; Xu, S.; Han, C.C. Multiple Targeted Drugs Carrying Biodegradable Membrane Barrier: Anti-Adhesion, Hemostasis, and Anti-Infection. Biomacromolecules 2013, 14, 954–961.

[21] Wu, J.; Zhang, Z.; Gu, J.; Zhou, W.; Liang, X.; Zhou, G.; Han, C.C.; Xu, S.; Liu, Y. Mechanism of a long-term controlled drug release system based on simple blended electrospun fibers. J. Control. Release 2020, 320, 337–346.

[22] Li, X.; He, Y.; Hou, J.; Yang, G.; Zhou, S. A Time-Programmed Release of Dual Drugs from an Implantable Trilayer Structured Fiber Device for Synergistic Treatment of Breast Cancer. Small 2019, 16, 1902262.

[23] Xu, L.; Li, W.; Sadeghi-Soureh, S.; Amirsaadat, S.; Pourpirali, R.; Alijani, S. Dual drug release mechanisms through mesoporous silica nanoparticle/electrospun nanofiber for enhanced anticancer efficiency of curcumin. J. Biomed. Mater. Res. Part A 2021, 110, 316–330.

[24] Sanoff, H.K.; Moon, D.H.; Moore, D.T.; Boles, J.; Bui, C.; Blackstock, W.; O'Neil, B.H.; Subramaniam, S.; McRee, A.J.; Carlson, C.; et al. Phase I/II trial of nano-camptothecin CRLX101 with capecitabine and radiotherapy as neoadjuvant treatment for locally advanced rectal cancer. Nanomed. Nanotechnol. Biol. Med. 2019, 18, 189–195.

[25] Seyedeh-Sara Hashemi, Amir Pakdin, Aliakbar Mohammadi, ACS Appl. Mater. Interfaces 2023, 15, 51, 59269–59279.

[26] Robert Wood and Gavin Taylor-Stokes, Cost burden associated with advanced non-small cell lung cancer in Europe and influence of disease stage (2019) 19–214.10.1186/s12885-019-5428-4.

[27] D.H. Truong, V.K. Hoa Le, T.T. Pham, A.H. Dao, T.P. Dung Pham, T.H. Tran, Delivery of erlotinib for enhanced cancer treatment: An update review on particulate systems, Journal of Drug Delivery Science and Technology (2019), doi: https://doi.org/10.1016/j.jddst.2019.101348.

[28] Parijat Pandey, Kamal Dua, Harish Dureja, ERN loaded chitosan nanoparticles: Formulation, physicochemical characterization and cytotoxic potential. International Journal of Biological Macromolecules, 139 (2019) 13041–316.10.1016/j.ijbiomac.2019.08.084.

[29] Duy Hieu Truong, Vu Khanh Hoa Le, Tung Thanh Pham,Anh Hoang Dao, Thi, Phuong Dung Pham, Tuan Hiep

Tran, Delivery of ERN for enhanced cancer treatment: An update review on particulate systems, Journal of Drug delivery Science and Technology. (2020), 31231–6.

[30] Sushant Lakkadwala, Jagdish Singh, Co-delivery of doxorubicin and ERN through liposomal nanoparticles for glioblastoma tumor regression using an in vitro brain tumor model, Colloids and Surfaces B: Bio Interfaces, (2019) 27–

[31] Sathyaraj Weslen Vedakumaria, Rethinam Senthila, Sathiya Sekard, Chidambaram Saravana Babue. Enhancing anti-cancer activity of ERN by antibody conjugated nanofibrin - In vitro studies on lung adenocarcinoma cell lines, Material chemistry and Physics,224 (2019) 328–333.

[32] Bray F, Ferlay J, Soerjomataram I, Siegel RL, Torre LA, Jemal A. Global cancer statistics 2018: GLOBOCAN estimates of incidence and mortality worldwide for 36 cancers in 185 countries. CA: a cancer journal for clinicians. 2018 Nov;68(6):394-424.

[33] Tran S, DeGiovanni PJ, Piel B, Rai P. Cancer nanomedicine: a review of recent success in drug delivery. Clinical and translational medicine. 2017 Dec;6:1-21.

[34] Bhuvaneshwar Vaidya, Vineela Parvathaneni, Nishant S. Kulkarni, Snehal K. Shukla, Jenna K. Damon, Apoorva Sarode, Dipti Kanabar, Jerome V . Garcia, Samir Mitragotri, Aaron Muth, Vivek Gupta , Cyclodextrin modified erlotinib loaded PLGA nanoparticles for improved therapeutic efficacy against non-small cell lung cancer. International Journal of Biological Macromolecules (2018),https://doi.org/10.1016/j.ijbiomac.2018.10.181.

[35] Shreya Thakkar, Dilip Sharma, Manju Misra, Comparative evaluation of electro-spraying and lyophilization techniques on solid state properties of ERN nanocrystals: Assessment of In-vitro cytotoxicity (2018) 257–269.10.1016/j.ejps.2017.10.008.

[36] Kyung Mi Yang, In Chul Shin, Joo Won Park, Kab-Sig Kim, Dae Kyong Kim, Kyungmoon Park, Nanoparticulation improves bioavailability ofERN (2017) 1557–1565.

[37] G. Paulos A, Yahya Mrestani B, Frank Heyroth C, Tsige Gebre-Mariam A, ,Reinhard H.H. Neubert B, D Fabrication Of Acetylated Dioscorea Starch Nanoparticles: Optimization Of Formulation And Process Variables Journal Of Drug Delivery Science And Technology 31 (2016) Page no. 83-92.

[38] Pérez-Herrero E, Fernández-Medarde A. Advanced targeted therapies in cancer: Drug nanocarriers, the future of chemotherapy. European journal of pharmaceutics and biopharmaceutics. 2015 Jun 1;93:52-79.

[39] E. F. Craparo, B. Porsio, M. L. Bond, G. Giammona ,G .Cavallaro, Evaluation Of Biodegradability On PolyaspartamidePolylactic Acid Based Nanoparticles By Chem Hydrolysis Studies. Polymer Degradation and Stability 119 (2015) Page no. 56-67.

[40] Wicki A, Witzigmann D, Balasubramanian V, Huwyler J. Nanomedicine in cancer therapy: challenges, opportunities, and clinical applications. Journal of controlled release. 2015 Feb 28;200:138-57.

[41] S. Tummala, M. N. Satish Kumar And Ashwati Prakash, Formulation And In Vitro Characterization Of Carbamazepine Polymeric Nanoparticles With Enhanced Solubility And Sustained Release For The Treatment Of Epilepsy, Journal Of Chemical And Pharmaceutical Research, 2015; 7(2): Page no.70-79.

[42] E. F. Craparo, B. Porsio, M. L. Bond, G. Giammona ,G .Cavallaro, Evaluation Of Biodegradability On Polyaspartamide Polylactic Acid Based Nanoparticles By Chem Hydrolysis Studies. Polymer Degradation and Stability 119 (2015) Page no. 56-67.

[43] Iravani S, Korbekandi H, Mirmohammadi SV, Zolfaghari B. Synthesis of silver nanoparticles: chemical, physical and biological methods. Res Pharm Sci. 2014 Nov-Dec;9(6):385-406.

[44] Y. Liua, C. Suna , Y. Haob, T. Jianga, Li Zhenga, S.Wanga, Mechanism Of Dissolution Enhancement And Bioavailability Of Poorly Water Soluble Celecoxib By Preparing Stable Amorphous Nanoparticles. J Pharm Pharmaceutsci (Www.Cspscanada.Org) 13(4) 2010; Page no. 589 – 606.

[45] Iravani S. Green synthesis of metal nanoparticles using plants. Green chemistry. 2011;13(10):2638-50.

[46] Y. Liua, C. Suna , Y. Haob, T. Jianga, Li Zhenga, S.Wanga, Mechanism Of Dissolution Enhancement And Bioavailability Of Poorly Water Soluble Celecoxib By Preparing Stable Amorphous Nanoparticles. J Pharm Pharmaceutsci (Www.Cspscanada.Org) 13(4) 2010; Page no. 589 – 606.

[47] Korbekandi H, Iravani S, Abbasi S. Production of nanoparticles using organisms. Critical reviews in biotechnology. 2009 Dec 1;29(4):279-306.

[48] Navaladian S, Viswanathan B, Varadarajan TK, Viswanath RP. Microwave-assisted rapid synthesis of anisotropic Ag nanoparticles by solid state transformation. Nanotechnology. 2008 Jan 4;19(4):045603.

[49] Kim D, Jeong S, Moon J. Synthesis of silver nanoparticles using the polyol process and the influence of

precursor injection. Nanotechnology. 2006 Jul 14;17(16):4019.

[50] Cozzoli PD, Comparelli R, Fanizza E, Curri ML, Agostiano A, Laub D. Photocatalytic synthesis of silver nanoparticles stabilized by TiO2 nanorods: A semiconductor/metal nanocomposite in homogeneous nonpolar solution. Journal of the American Chemical Society. 2004 Mar 31;126 (12):3868-79.

[51] Becker ML, Bailey LO, Wooley KL. Peptide-derivatized shell-cross-linked nanoparticles. 2. Biocompatibility evaluation. Bioconjugate chemistry. 2004 Jul 21;15(4):710-7.

[52] Sastry M, Ahmad A, Khan MI, Kumar R. Biosynthesis of metal nanoparticles using fungi and actinomycete. Current science. 2003 Jul 25:162-70.